ABSTRACT

Vertical scanning interference microscope measurements of the mean radius of curvature (ROC) of both surfaces of constant-volume, deformable, water-filled lenses were obtained before and during small displacement stepped equatorial stretching in the plane perpendicular to the optical axis. Each lens demonstrated a marked decrease of the ROC at its optical center. However, the ROC increased in a region halfway between the center and the outer diameter of the lens. This is indicative of central steepening with peripheral flattening. This is contrary to the assumption that stretching of the equator of a deformable lens will only reduce its optical power.

ORIGINAL ARTICLE

Paradoxical Optical Power Increase of a Deformable Lens by Equatorial Stretching

Ronald A. Schachar, MD, PhD, Donald P. Cudmore, MS, Truman D. Black, PhD, James C. Wyant, PhD, Victor W. Shung, MS, Tseng Huang, PhD, Ryan T. Mckinney, BS, & Jannick P. Rolland, PhD

Recently, it has been suggested that small displacement equatorial stretching of a biconvex deformable lens actually produces central steepening with a large increase in optical power,[1] contrary to prior assumptions.[2,3] To test this hypothesis, a vertical scanning interference microscope[4,5] was used to measure the mean radius of curvature of the surfaces of deformable lenses during small displacement equatorial stretching.

Each of four transparent, constant-volume, water-filled, biconvex deformable lenses (Fig 1a) were suspended in the center of a ring by clamping their equatorial lip to eight equally spaced opposing micrometers with nonrotating spindles (Fig 1b). The ring with the attached lens was placed on the stage of a vertical scanning interference microscope (RST Plus, WYKO Corporation, Tucson, AZ) (Fig 1c). A vertical scanning interferometer was selected for the measurement because it provides a good way of measuring both radius of curvature and changes in the radius of curvature without any ambiguity in the sign. In the vertical scanning interferometer, an unfiltered white- light source is used. Due to the large spectral bandwidth of the source, the coherence length of the source is short, and good contrast fringes are obtained

Reprints:

Ronald A. Schachar, MD, PhD, Presby Corp, PO Box 796728, Dallas, TX 75379.

Dr. Schachar and Mr. Cudmore are from Presby Corp, Dallas, Texas. Dr. Black is from the Department of Physics, University of Texas at Arlington, Arlington, Texas. Dr. Wyant is from the Optical Sciences Center, University of Arizona, Tucson, Arizona. Mr. Shung and Dr. Huang are from the Department of Mechanical Engineering, University of Texas at Arlington, Arlington, Texas. Mr. Mckinney is from Parametric Technology Corporation, Dallas, Texas. Dr. Rolland is from the Center for Research and Education in Optics and Lasers, University of Central Florida, Orlando, Florida.

Acknowledgments

The authors would like to thank Jeffrey T. Brown and Tami L. Batler of WYKO Corporation, Tucson, AZ 85706, for operating the vertical scanning interference microscope.

Fig 1a.—Photograph of a water-filled deformable lens in the center of a teething ring. The water-filled deformable lenses were made from transparent teething rings that did not have the imprinted design.

Fig 1b.— Photograph of a water-filled deformable lens mounted in the center of a ring by clamping its equatorial lip to eight, equally spaced, opposing micrometers with nonrotating spindles.

only when the two paths of the interferometer are closely matched in length. Thus, if in the interference microscope the path length of the sample arm of the interferometer is varied, the height variations across the sample can be determined by looking at the sample position for which the fringe contrast is maximum. In this measurement, the height ambiguities that can be present if a quasi-monochromatic light source is used are eliminated.[4,5]

Materials & Methods

Four transparent, constant-volume, water-filled, biconvex deformable lenses, with a wall thickness of 0.5 mm were made by cutting out individual balloon elements of transparent water-filled polyvinylchloride teething rings (Safety lst, Chestnut Hill, MA). The balloon element was heat sealed around its periphery to leave a closed, biconvex cross-section lens envelope

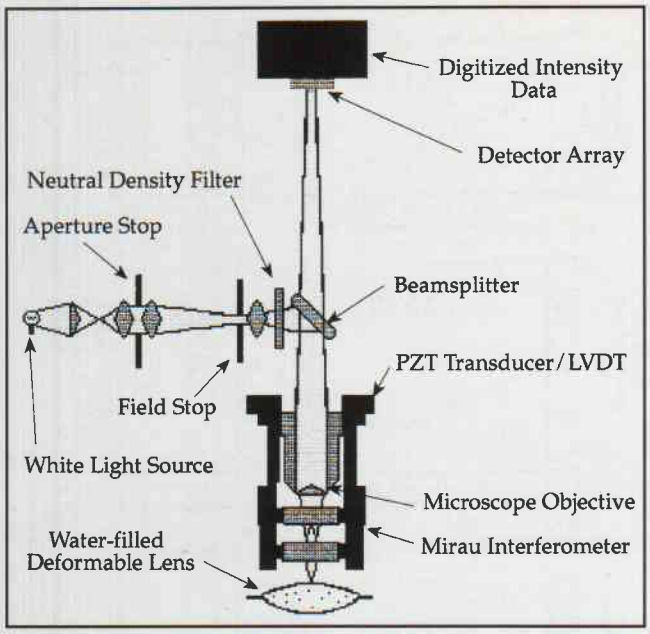

Fig 1c.—Schematic diagram of the vertical scanning interference microscope, WYKO Corporation, model RST Plus.

with a 1.0 mm thick lip extending approximately 6.0 mm around the entire equator (Fig 1a). The lenses were then filled with water, using a hypodermic needle whose entrance holes were sealed by heating. All of the resulting lenses had approximately the same equatorial diameter: 25.3 ± 0.5 mm. Their central thicknesses were 11.95, 8.41, 11.07, and 6.50 mm, respectively.

The magnification of the interference microscope objective was selected so that the interferometer measures over a 3.68 x 2.68 mm area centered on a point on the surface of the lens. The resolution was 6 microns laterally and 3 nanometers vertically. Using a least squares parabolic fit, a mean radius of curvature (ROC) was calculated for the entire selected area. The ROC was obtained at the optical center of each lens surface. Each of three lenses was stretched at its equator by turning each micrometer outwardly a total of 0.252 mm in four equal 0.063 mm increments. Then, the direction was reversed in four 0.063 mm increments. This process was repeated three times for each surface. The ROC was measured after each incremental expansion of equatorial diameter and after each incremental relaxation, using the vertical scanning interference microscope.

In addition, in Lens 4, measurements of the ROC were made of both surfaces at the optical center, and at 3 mm and 6 mm from the optical center. These measurements were made before and after the micrometers were turned outwardly 0.178 mm.

Independently, a finite element analysis of an unstretched deformable lens similar to Lens 4 was modeled. The measured ROCs of the back surface of Lens 4 (Fig 3b) in the unstretched state were used. This segment of lens profile was best fit to a fourth-order polynomial equation:

$$y = 6 - (a_1 x^2 + a_2 x^3 + a_3 x^4)$$

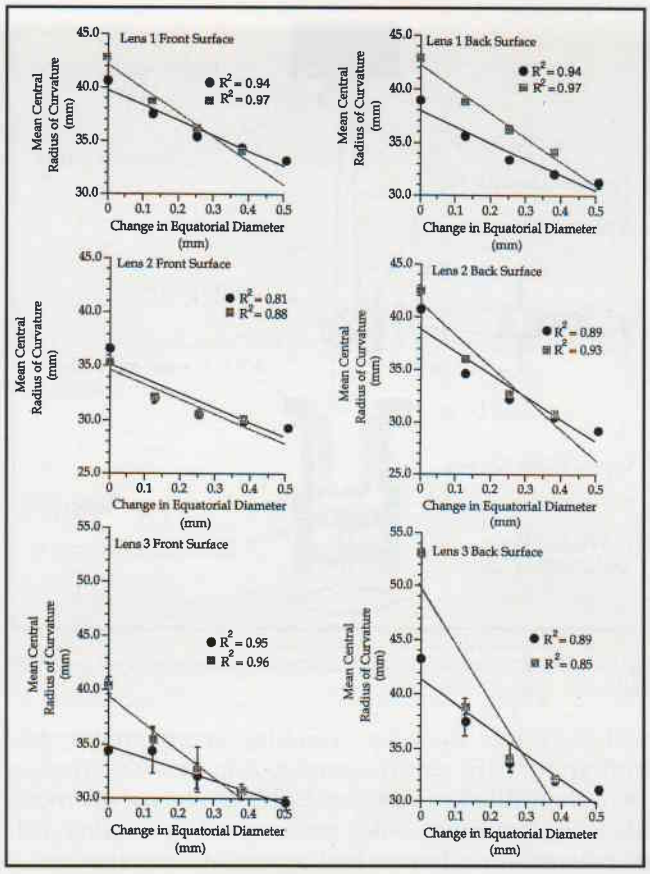

Fig 2a.—Plot of the mean of three measurements of the ROC, measured by the vertical scanning interference microscope, of the front and back surfaces of three water-filled deformable lenses versus their change in equatorial diameter for stretching (●) and relaxation (▩) back to their initial equatorial diameters. Note that equatorial stretching produced central steepening. The least squares line is shown. R^2 is the square of the linear correlation coefficient.

The three coefficients of the equation were obtained from the following three conditions:

@ x = 0 mm; r_1 = 43.56 mm

@ x = 3 mm; r_2 = 41.89 mm

@ x = 6 mm; r_3 = 27.17 mm

where the equation for the radius of curvature is:

$$\frac{1}{r_i} = \frac{|y_i''|}{[1+(y_i')^2]^{1.5}}$$

The mathematical lens profile was obtained by solving the above nonlinear equations. The coefficients were found to be:

a_1 = 0.0114784

a_2 = -0.0003031576963475039

a_3 = 0.00006050020561257952

The profile of the lens surface beyond 6 mm off center was drawn from visual inspection of the lens. For this analysis, the lens was assumed to be symmetrical, with an equatorial diameter of 25.4 mm and a thickness of 12.0 mm (Fig 4a).

The material properties of the polyvinylchoride shell were obtained from the strength tests performed by GenCorp. A summary of the stress-strain relationships are shown in Table 1. The Poisson's ratio was determined by the authors through a uniaxial tension test.

The material properties of water were simulated by using Mooney-Rivlin constitutive law[6,7] and are given

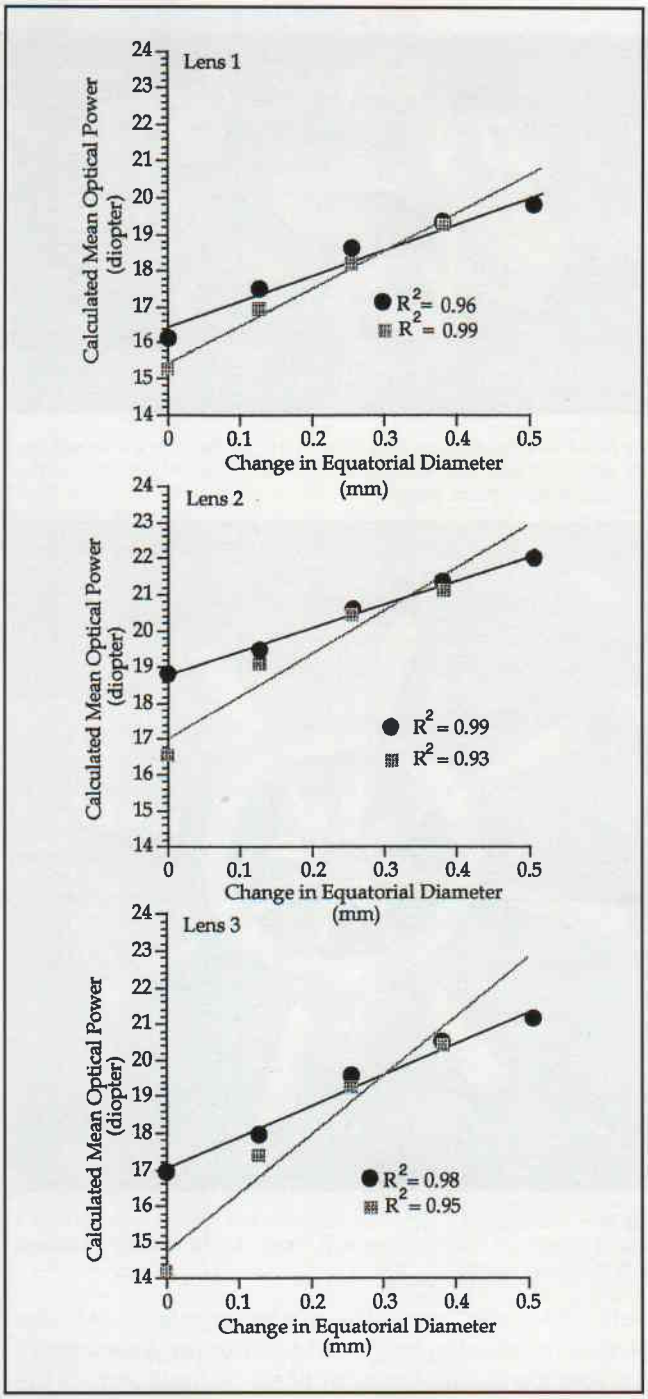

Fig 2b.— Plots of the calculated mean optical power versus change in equatorial diameter for stretching (●) and relaxation (▩) back to their initial equatorial diameters. The least squares line is shown. R2 is the square of the linear correlation coefficient.

as follows:

$$W = A(T_1 - 3) + B(T_2 - 3) + \beta(T_3^2 - T_3^{-2})^2$$

where

T_1 = reduced strain invariants in the i^{th} direction, which are given by :

$T_1 = I_1 I_3^{-1/3}$

$T_2 = I_2 I_3^{-2/3}$

$T_3 = I_3^{1/2}$

A, B = Mooney-Rivlin material constants where

$$\beta = \frac{(1+\nu)}{(1-2\nu)} \frac{A+B}{24}$$

TABLE 1

Stress-Strain Data for Polyvinylchoride

Strain, ε	0.0000	0.1667	0.5000	0.8333	1.3333	2.3333
Stress, σ (N/mm²)	0.0000	4.5505	9.8595	12.7035	15.4534	18.7372

Poisson's ratio, ν = 0.411

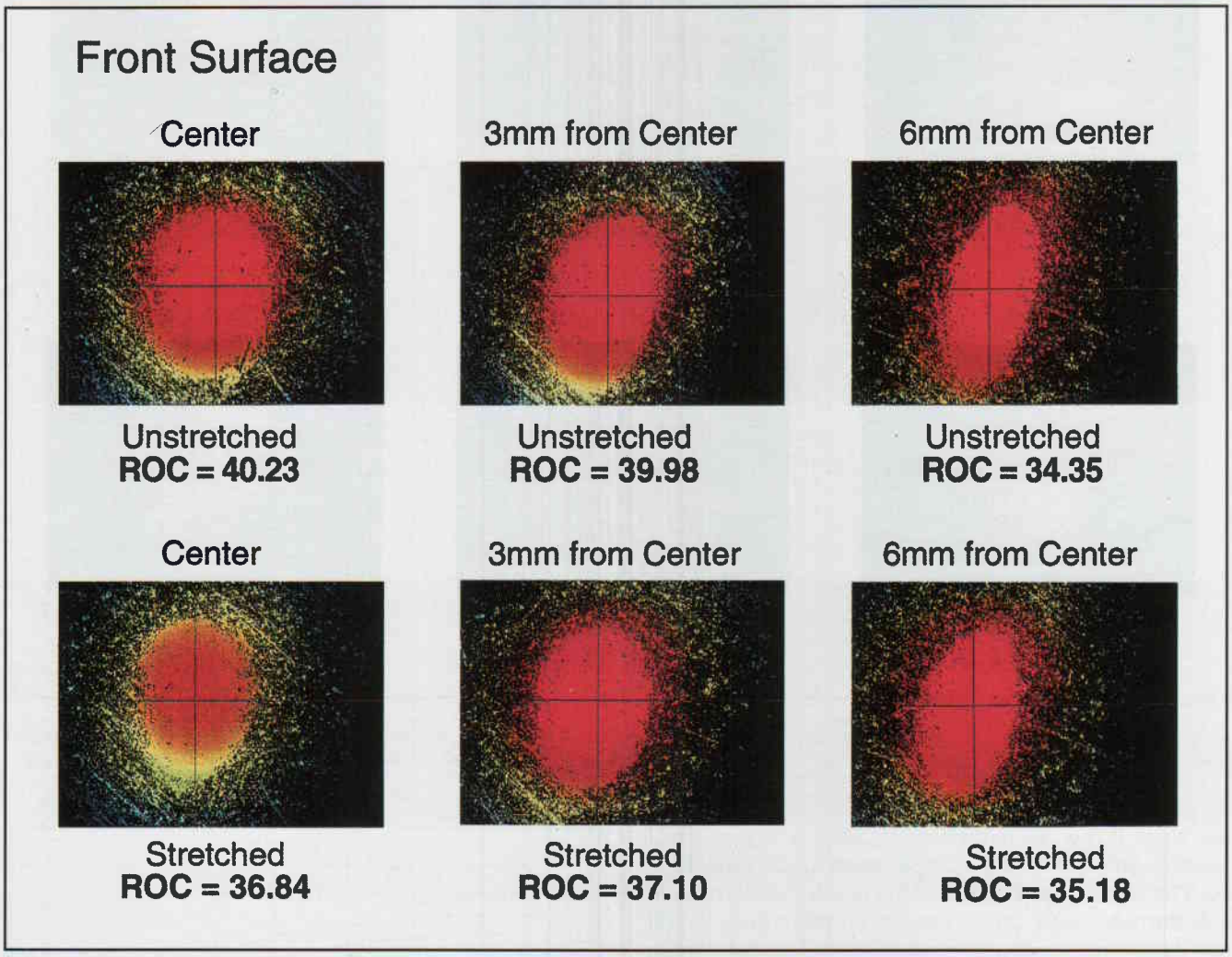

Fig 3a.—Vertical scanning interference microscope contour maps of the front surface of Lens 4. Red represents the high points and blue the low points. The ROC is given in millimeters at the center, at 3 mm, and at 6mm from the center. The equatorial stretching of the water-filled deformable lens resulted in central steepening with peripheral flattening.

ν = Poisson's ratio

I_1 = invariants of the right Cauchy-Green deformation tensor C_{ij}

$I_1 = C_{ii}$

$I_2 = ½ (I_1^2 - C_{ij} C_{ij})$

I_3 = Det C_{ij} = volume change ratio

Therefore, A, B, and ν were the only three material constants for the HYPER84 element.

To simulate water, the hyperelastic element must satisfy three distinct characteristics. First, the hyperelastic element must be very flexible under uniaxial loading while there is no confinement in the other directions perpendicular to the loading direction. Second, the element must have a very small shearing resistance so that its shape can be changed easily. Third, the element must be able to maintain a constant volume so it can sustain pressure when it is under a total 3-D confined environment. In other words, the bulk modulus must be large. These characteristics can be accomplished by assigning an extremely small value to the Mooney-Rivlin constants (A and B) and a Poisson's ratio approaching 0.5. Since for small strains, the shear modulus and the Young's modulus can be approximated as 2•(A+B) and 6•(A+B), respectively and the bulk modulus can be represented as 2•(A+B) / (1-2•ν). If both constants A and B are small, the shear modulus and Young's modulus will also be small. The bulk modulus is not solely dependent on constants A and B; it is also dependent on Poisson's ratio. If Poisson's ratio approaches 0.5, the bulk modulus can still

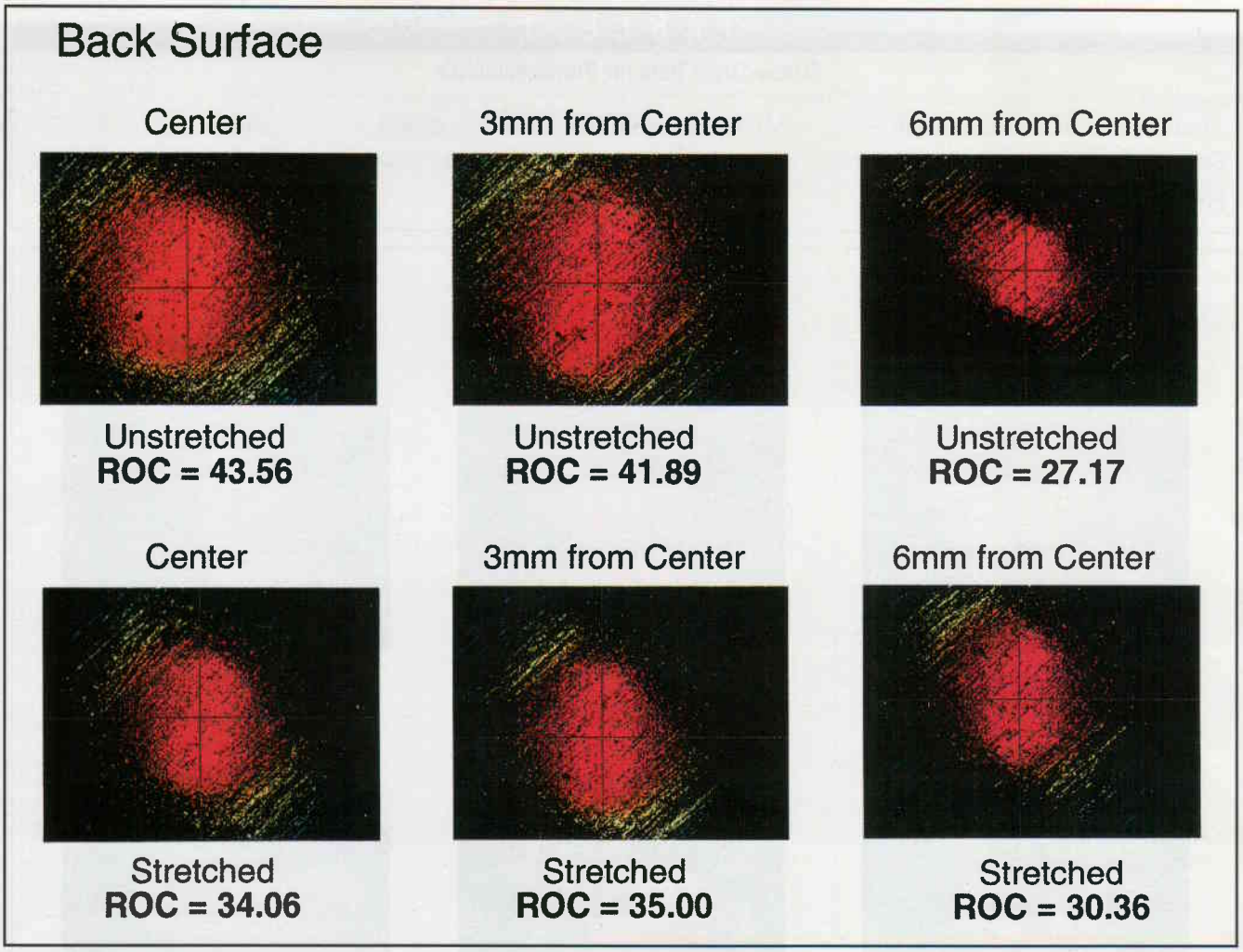

Fig 3b.—Vertical scanning interference microscope contour maps of the the back surface of Lens 4. Red represents the high points and blue the low points. The ROC is given in millimeters at the center, at 3 mm, and at 6mm from the center. The equatorial stretching of the water-filled deformable lens resulted in central steepening with peripheral flattening.

be very large. A computer model using several Mooney-Rivlin constants and Poisson's ratios was tested. The results indicated that the stress distribution of a deformable lens under equatorial stretching would not have any significant change if the Mooney-Rivlin constants were limited to under 0.0003. Therefore, in this analysis, water was represented by Mooney-Rivlin constants A = B = 0.0003 N/mm², ν = 0.499999, and a bulk modulus = 600 N/mm².

The finite element model was constructed using ANSYS 5.3, a general-purpose finite element program.[6,7] Due to the symmetrical nature of the geometry and loading, a 2-D axisymmetrical model was used for the analysis. The deformable lens, made of polyvinylchloride, was modeled using a PLANE82 element. This 2-D eight-node quadrilateral element had two degrees of freedom at each node: translation in the nodal x and y directions. Three layers of elements were used through the thickness of the lens, which provided a total of seven nodal points across the thickness. This allowed the shell to form a smooth parabolic displacement shape. Due to the nonlinear stress-strain material properties, a material data table was established to define its material properties at different stress levels. The constant volume liquid filling the lens was modeled using a HYPER84 element. This 2-D, eight-node Hyperelastic quadrilateral element had two degrees of freedom at each node: translation in the nodal x and y direction. The axisymmetric option had an additional degree of freedom at each node: transla-

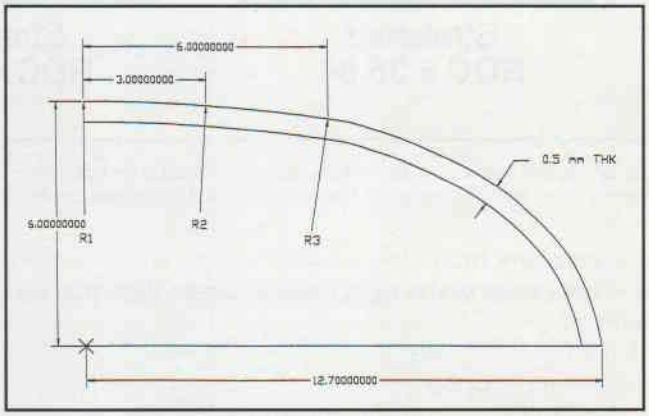

Fig 4a.—Geometric model of the deformable lens used for the finite-element analysis.

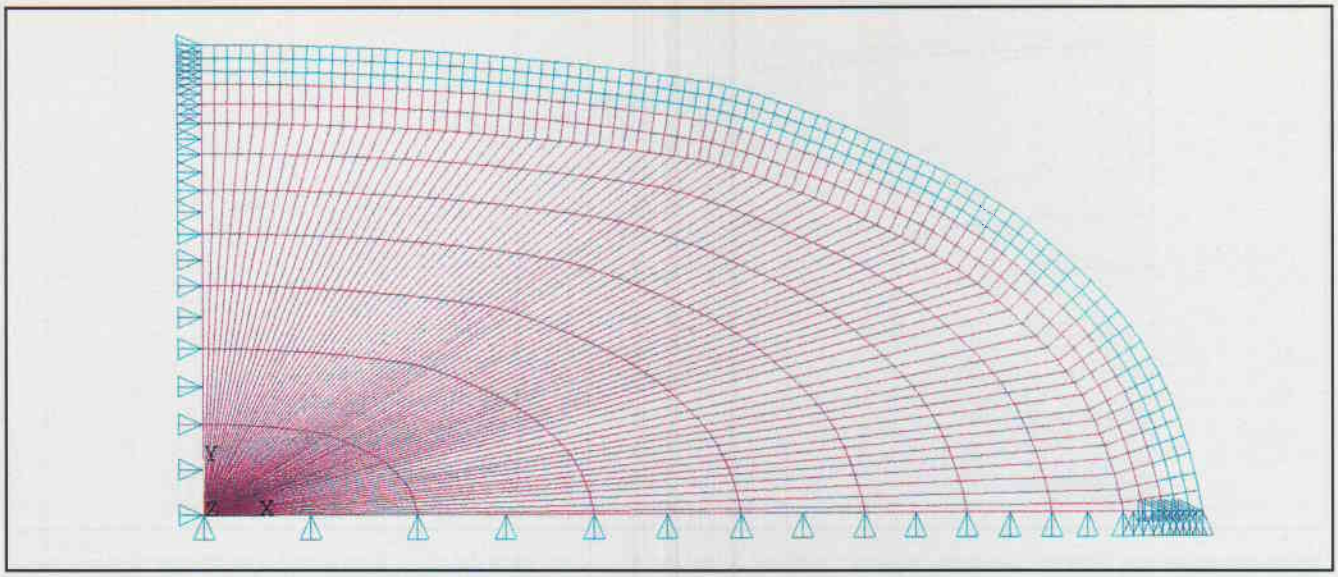

Fig 4b.—The boundary conditions using Ansys 5.3 of the finite-element model.

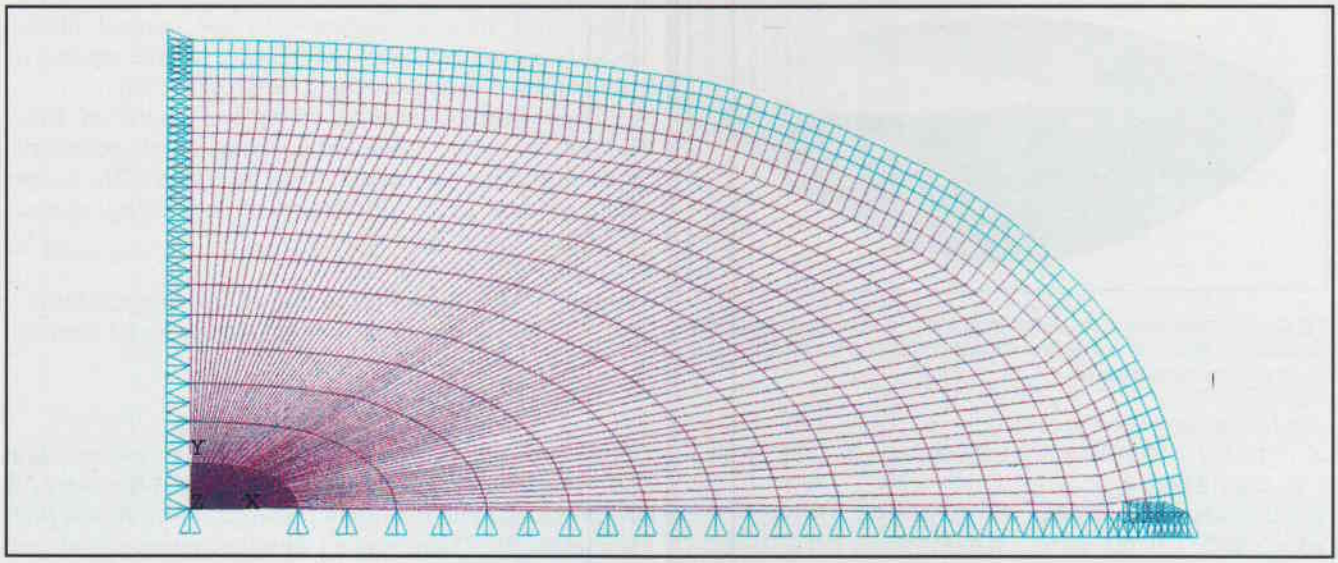

Fig 4c.—The boundary conditions of the finite-element model when the mesh density for water was doubled.

tion in the z direction, allowing torsion in the model. However, the torsion mode was eliminated in this analysis because of its symmetrical nature. Also, a 2-D 6-node Hyperelastic triangular element was used in a few locations, as needed. Note that only two layers of fine elements were generated near the surface of the Hyperelastic element; the rest of the elements were coarse (Fig 4b). Because we were not interested in the stress distribution in the water, the Hyperelastic elements were treated as boundary control devices to obtain a constant volume inside the shell. The possible error caused by the mesh density was examined by doubling the number of the Hyperelastic elements (Fig 4c). Geometric nonlinearity must be included in the computation because of the relatively large displacements that may occur in the deformation. By using the Mooney-Rivlin strain energy density function, a nearly incompressible material was modeled.

A diagram of the boundary conditions for the model are shown in Fig 4a–4c. As shown in the figures, the symmetry boundary conditions were applied along the x and y axes. In order to eliminate the torsion mode, a displacement constrain of UZ was applied to all HYPER84 elements. A total of 0.356 mm of horizontal displacement in the + x axis direction was imposed along the equator in order to simulate stretching. Since the solution was highly nonlinear (it involves both nonlinearity of the geometric and material properties), a discrete load step was applied to ensure convergence of the solution.

An independent geometric element analysis was used to analyze a solid deformable lens of the same shape and size as the human crystalline lens (Fig 4e). The profiles of the anterior and posterior surfaces of a human crystalline lens with a diameter of 8.6 mm were best fit to fifth polynomials.[8]

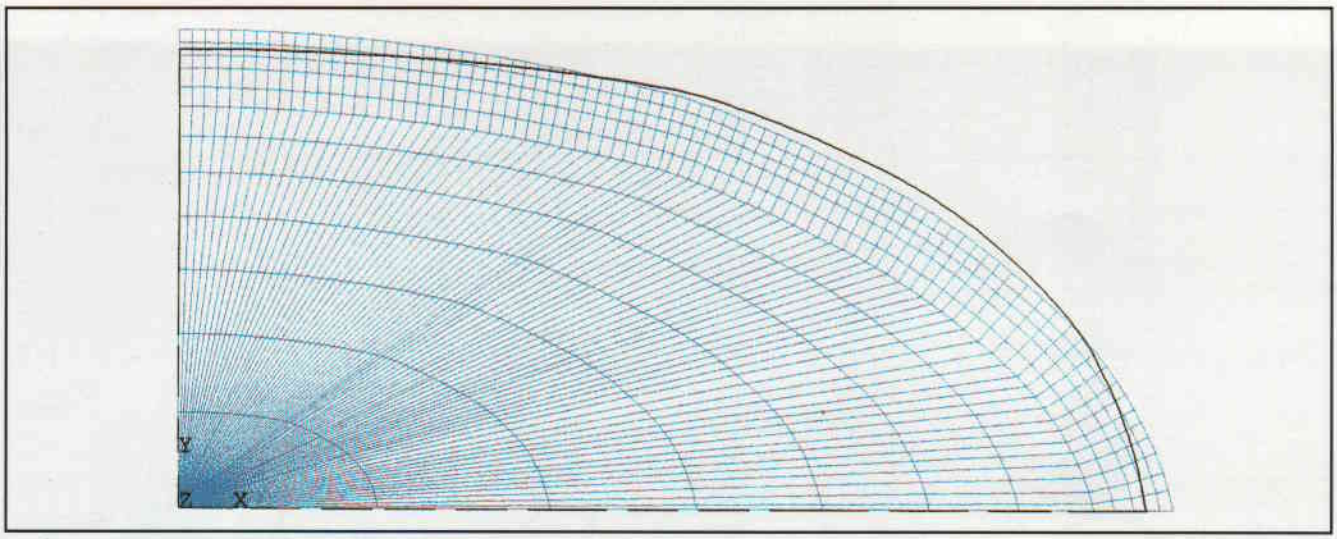

Fig 4d.—The displacement plot of the finite-element model for a maximum displacement of 0.356 mm with a scale of 1:1. The blue mesh is the deformed state as a result of equatorial stretching. The black line is the unstretched state.

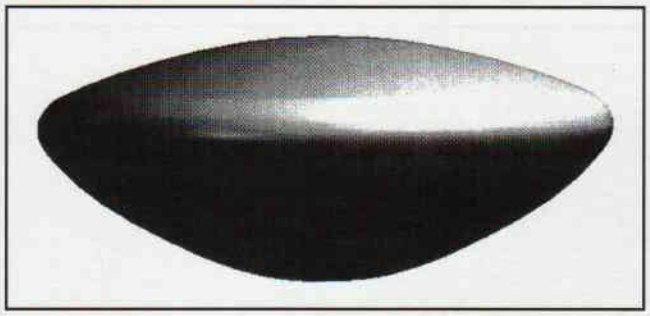

Fig 4e.—Computer image of the solid polyvinylchloride model created from the 5th polynomials of the anterior and posterior surfaces of the human crystalline lens used for the geometric element analysis.

For the anterior surface:

$z_a = 1.3727\text{-}0.373134\ x^2 - 0.0259909\ x^3 + 0.0102632\ x^4 - 0.00123879\ x^5$

For the posterior surface:

$zp = 2.3373 - 0.053191\ x^2 - 0.032101\ x^3 + 0.032101\ x^4 - 0.0039910\ x^5$

Pro-Engineer software with the Mechanica module was used to model the effects of 80μ of equatorial stretching of a solid piece of polyvinylchloride with the same dimensions and shape as the human crystalline lens. A Young's modulus of 3000N/mm² and a Poisson's ratio of 0.4 were used for this analysis.

A computer calculation of the spherical aberration of Lens 4 was made using a 10th order equation for an aspheric surface:

$$z = [Cp^2/1 + \sqrt{1-(1+k)c^2p^2}] + \alpha_1p^2 + \alpha_2p^4 + \alpha_3p^6 + \alpha_4p^8 + \alpha_5p^{10}$$

where: Z is the sag, C is the curvature of the surface at the apex, p is the normalized height on the lens with respect to the effective diameter of the lens (i.e., 15 mm in this case), and k = 0. The α coefficients are given in Table 2.

Results & Discussion

The means of the three measurements of the central ROC, from both surfaces of each lens, are plotted in Fig 2a. There was a marked decrease in the central ROC, and thus an increase in the central optical power, associated with stretching of the equatorial diameters of the water-filled deformable lenses.

The effective increase in optical power of these lenses for each incremental change with equatorial stretching was calculated. Each interface of the lenses was treated as an independent refracting surface using the Gaussian formula:[9]

$$n/s + n'/s' = (n'-n)/r$$

where: n = index of refraction of the first medium
n' = index of refraction of the second medium
s = object distance
s' = image distance
r = mean ROC of each surface

The indexes of refraction of air, water, and polyvinylchloride were taken to be 1.00, 1.33, and 1.55, respectively. The results of these calculations are plotted in Fig 2b. There was a 1 diopter increase in optical power for each 0.109 ± 0.035 mm of equatorial stretching. This is comparable to the measured change in optical power reported for small-displacement equatorial stretching, 1 diopter/0.1 mm, of similar water-filled deformable lenses.[1] The surfaces of Lens 4 steepened during equatorial stretching at the optical center and 3 mm from the optical center but flattened at 6 mm from the optical center (Fig 3a).

The deformed shape for the water-filled deformable lens under a 0.356 mm stretching of the equator as predicted by the finite element analysis is shown in Fig 4d. The plot indicates that the volume of the lens increases centrally. These results may look strange at first. However, the fact is that the volume increase at the periphery of the lens due to the stretching is less than the reduction in volume of the middle section of the lens. On the other hand, since the volume under the shell still remains constant, the extra volume must go somewhere else. The center of the lens, which is furthest from the boundary, seems to be the most vulnerable place for inheriting the extra volume.

TABLE 2

α Coefficients for 10th Order Equation

Coefficients	Unstretched Water-Filled Lens		Stretched Water-Filled Lens	
	Front surface	Back surface	Front surface	Back surface
α_1	5.00417E-06	-1.45961E-05	1.3767E-06	4.1364E-06
α_2	-4.8926E-06	1.0174E-05	-3.3299E-06	7.8600E-07
α_3	3.56267E-07	-1.0341E-06	1.04037E-07	2.4961E-07
α_4	-1.0837E-08	3.0894E-08	-3.7102E-09	-3.89432E-09
α_5	1.13529E-10	-3.17657E-10	4.48576E-11	-9.61766E-13
ROC	40.23 mm	43.56 mm	36.84 mm	34.06 mm

TABLE 3

Calculated Radii of Curvatures of the Water-Filled Deformable Lens

Distance from the center	0 mm	3 mm	6 mm
Radii of curvatures of the unstretched lens	43.56 mm	41.89 mm	27.17 mm
Calculated radii of curvatures after equatorial stretching	24.93 mm	25.61 mm	37.92 mm
Calculated radii of curvatures after equatorial stretching (using double the mesh density for water)	24.91 mm	25.60 mm	37.92 mm

The radius of curvature at the surface of the lens is calculated using a finite difference method. It should be noted that the change of the radius of curvature, which involved the second derivative of the displacement function, was very sensitive to a numerical truncated error. Therefore, eight digits of numerical accuracy were used throughout the analysis. Furthermore, the first and second derivatives calculated by the finite difference method has an error of $(o)h^6$, where h (h = ⅛ mm) is the interval. The calculated radii of curvatures before and after stretching are given in Table 3. There was essentially no effect on the calculated radii of curvatures by increasing the mesh density for water.

One other concern of this finite element analysis was the numerical error that may occur because of the significant difference between the modulus of elasticity of polyvinylchloride and water. In order to minimize this error, which would occur from the shear stress not being transferred correctly between the surfaces of the two materials, we used very fine elements at the transition area.

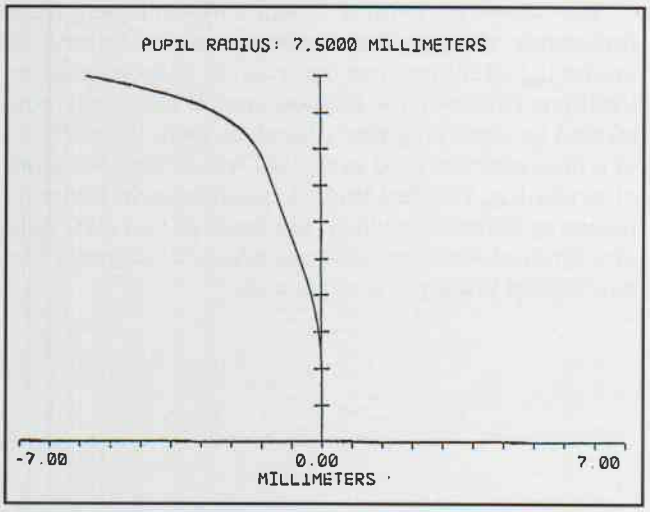

Fig 5a.—A plot of the longitudinal aberration of the unstretched water-filled deformable lens.

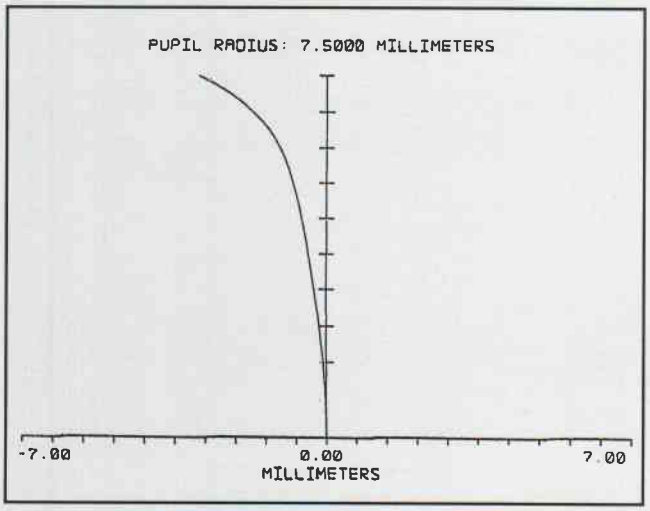

Fig 5b.—A plot of the longitudinal aberration of the stretched water-filled deformable lens.

The geometric element analysis predicted that the behavior of the solid deformable lens mimics that found with the water-filled deformable lens during small-displacement equatorial stretching (Table 4).

The computer calculation of optical ray tracing through Lens 4 demonstrated that equatorial stretching reduced its spherical aberration (Fig 5). The longi-

TABLE 4

Calculated Radii of Curvatures of the Solid Deformable Lens

	Distance from the Center	0	1.37 mm	2.75 mm
Radii of curvatures of the anterior surface	Unstretched state	13.40 mm	9.10 mm	12.84 mm
	Stretched state	7.76 mm	8.28 mm	14.39 mm
Radii of curvatures of the posterior surface	Unstretched state	9.40 mm	4.94 mm	8.93 mm
	Stretched state	3.40 mm	5.00 mm	10.97 mm

tudinal spherical and wave-front aberrations decreased from -5.6 mm and 44 waves to -3.15 mm and 38 waves, respectively.

The observed central steepening and peripheral flattening during small-displacement equatorial stretching of a biconvex deformable body is counterintuitive. However, the phenomenon is readily demonstrated by observing the reflections from the surfaces of a biconvex air-filled mylar balloon during equatorial stretching. The fact that the phenomenon occurs in biconvex structures, which are made of two materials, or a solid, which is made of one material, suggests that a universal principle is applicable.

References

1. Schachar RA, Cudmore DP, Black TD. A revolutionary variable focus lens. *Ann. Ophthalmol.*1996;28:11–18.
2. Bennett AG. Variable and progressive power lenses: 2. *Optician.*1970;160,533–538.
3. Sullivan CM, Fowler CW. Progressive addition and variable focus lenses: A review. *Ophthal. Physiol. Opt.*1988:8;402–414.
4. Caber PJ. Interferometric profiler for rough surfaces. *Appl. Opt.*1993;32:3438–3441.
5. Wyant JC. Computerized interferometric measurement of surface microstructure. *Proc. SPIE* 1995;2576:122–130.
6. ANSYS 5.3. *User's Manual.* Houston, Pennsylvania: Swanson Analysis Systems, Inc; 1996.
7. ANSYS 5.3. *Theory Reference.* Houston, Pennsylvania: Swanson Analysis Systems, Inc.; 1996.
8. Schachar RA, Huang T, Huang X. Mathematic proof of Schachar's hypothesis of accommodation. *Ann Ophthalmol.*1993;25:5–9.
9. Born M, Wolf E. *Principles of Optics.* 4th ed. Oxford, England: Pergamon; 1970:161–163.